Lab on a Chip

Progressive Sperm Separation Using Parallelized, High-Throughput, and Efficient Microchamber-based Microfluidics

Journal:	*Lab on a Chip*
Manuscript ID	LC-ART-02-2021-000091.R1
Article Type:	Paper
Date Submitted by the Author:	24-May-2021
Complete List of Authors:	Yaghoobi, Mohammad; Cornell University, Azizi, Morteza; Cornell University Mokhtare, Amir; Cornell University College of Agriculture and Life Sciences, Abbaspourrad, Alireza; Cornell University, Food Science; Cornell University

Progressive Bovine Sperm Separation Using Parallelized Microchamber-based Microfluidics

*Mohammad Yaghoobi, Morteza Azizi, Amir Mokhtare, Alireza Abbaspourrad**

M.Y. Author 1, M.A. Author 2, A.M. Author 3, A.A. Author 4

Food Science Department, College of Agriculture and Life Sciences, Cornell University, Ithaca, NY 14853-5701, USA.

E-mail: **alireza@cornell.edu**

Keywords: sperm separation, high-throughput, efficiency, microfluidics, progressive motility

Abstract

Motility is one of the most important factors in sperm migration toward an egg. Therefore, sperm separation based on motility might enhance sperm selection for infertility treatments. Conventional centrifugation-based methods increase the risk of damage to sperm cells. Microfluidic systems, on the other hand, can sort sperm in a less intrusive way, but their efficiency and throughput still needs improvement, especially in low-concentration samples (oligozoospermia). Here, a microchamber-based microfluidic platform is demonstrated that can separate progressively motile sperm from non-viable sperm and debris, and trap nonprogressive sperm in microchambers. This platform can be operated in a short period of time (<10 min) with an excellent degree of controllability with no sample preparation. Sperm were screened in a 384-microchamber platform. The mean average-path velocity of the motile sperm in the collected sample increased significantly, from 57±10 μm/s in the raw semen sample to 81±13 μm/s. The DNA Integrity of the separated sperm showed 20% improvement over the raw sample which indicated that separated sperm were of higher quality. We began with a 22.5 μL

raw bovine sperm sample which had a concentration of 8.5 million sperm per milliliter (M mL^{-1}) with 38% motility. After separation, the concentration of the collected sperm was 2.1 M mL^{-1} with a motility rate of 90%. This corresponds to an 75% retrieval efficiency and the selection of approximately 5.2 x 10^4 progressively motile spermatozoa. Our results show that the microchamber depth does not affect the residence time of motile sperm; therefore, it is possible to inspect higher sample volumes within the same time frame. This microfluidic platform may provide an easy-to-implement solution for high-throughput, robust, and efficient, collection of progressive sperm with the DNA integrity needed for assisted reproductive technologies (ARTs). However, further studies are necessary to show the implications of this method in human cases

1. Introduction

Sperm quality is central to the success of ART, as it can directly alter fertilization outcomes and offspring health.(1, 2) Sperm separation plays a crucial role in improving sperm quality, in both research and clinical settings, to facilitate discovery of the underlying factors that cause infertility. DNA integrity,(3) hyaluronic acid-binding capability,(4) progressive motility, morphology,(5) capacitation ability,(6) and plasma membrane negative charge(7) are among the sperm characteristics that have been evaluated to date. Among these, progressive motility is a critical factor that enables sperm to pass through barriers in the female reproductive tract.(8, 9)

Conventional methods of sperm separation, which focus mostly on sperm motility, involve density gradient centrifugation and swim-up.(1) However, these methods have detrimental effects on a sperm's genetic load(10, 11) and increase the rate of apoptosis in infertile sperm.(12) This shows both the flaws inherent to these methods and the sensitivity of sperm from infertile men compared with sperm from fertile men. In addition, these methods require highly technical skills, lack standardized procedures, and are prone to human error, not

to mention that they are time consuming.(1) In response, emerging technologies, such as microfluidics, have been examined as promising remedies that can not only alleviate the flaws involved in conventional methods of gamete preparation but also improve outcomes.(2, 13-21)

Motile mammalian sperm can undergo rheotaxis,(22) follow boundaries,(18, 23, 24) or cross streamlines.(17, 25) The bulk of motile sperm can also move around within the environment on random paths.(14) These characteristics have been utilized in various microfluidics platforms to separate motile sperm. Cho et al.(17) were the first researchers to introduce the crossing of streamlines for sperm separation in microfluidics. Recently Gai et al. improved on that design by adding acoustic transducers to increase output.(26) In another attempt, Phiphattanaphiphop et al.(27) used design of experiment (DOE) and optimization to improve the efficiency of the same method for separating bull spermatozoa. Their results show 95% motility; however, the procedure requires extended time and sample preparation. Phiphattanaphiphop et al. reported using 5000 rpm centrifugation to separate egg-yolk extenders. This additional step may itself inflict damage on sperm cells.

Rheotaxis, which is a passive, hydrodynamically controlled process,(28) was used in a diffuser-type microfluidics device to select motile sperm.(29) It has been used to isolate motile sperm in a coral which can be tuned to the velocity of separated sperm.(13) These methods rely for the most part on highly concentrated sperm samples to be effective.

Apparent random motion of sperm in a quiescent medium has been guided within space-constrained microfluidic channels to separate racing sperm;(30) this method is more suitable for separation with intracytoplasmic sperm injection (ICSI) process using a low concentration of highly motile samples (80%).

One particular motility-based sperm separation technique provides loaded sperm with gate/guide channels through which motile sperm navigate to an outlet. Asghar et al.(14) loaded a sample of 0.56 mL into a chamber covered with a membrane with pores of 3-8 μm in diameter. Their results show significant improvement in motility (from 46% to 95%) with ~40% retrieval

efficiency. Because of the small size of pores in the membrane, however, this process takes nearly 45 minutes to complete. Nosrati et al.(18) loaded 1 mL of semen into 500 parallel channels with a 100×75 μm^2 cross-section. In their design, there is a much better opportunity to collect motile sperm with nearly 100% vitality as a result of the wider escape gaps and guiding paths, but the cumulative area of gaps per loaded volume is far less than Asghar et al. (14) leading to a relatively low concentration of separated sperm (6.32 M mL^{-1}) compared with the concentration of raw semen (120 M mL^{-1}).

Sperm separation time is an important factor, as it can compromise sperm motility, viability, and DNA integrity if takes more than 2 hours.(31) Reducing the time during which sperm separation occurs has been proven to have a positive impact on ICSI outcomes.(32) Furthermore, dead and apoptotic sperm in the sample generate reactive oxygen species (ROS) which induce apoptosis in the motile sperm affecting their motility.(33) One estimation of a processing time that has a minimal effect on viability is 10 minutes for processing a 1 mL sperm sample.(1) However, sperm separation for low-concentration samples requires more efficient methods that can be operated in lesser time. To the best of our knowledge, none of the previous methods that have used sperm motility for sperm separation have met these criteria for raw, low-concentration samples in an efficient manner. (13-15, 17, 18, 25, 27, 30)

Separation efficiency becomes very important in the case of oligozoospermia and that is another factor that centrifugation methods fall short of satisfying.(7, 25) To increase efficiency and reduce separation time, we designed a microchamber-based microfluidics platform to dramatically increase the gap size (entrance of the microchambers) per volume of loaded sample. This platform uses the boundary-following ability of progressively motile sperm for separation, with the least possible invasiveness. An equilibrium condition is reached in the microchambers after loading, which is stable with varying concentrations of loaded samples. The efficiency of the various microchamber diameters are evaluated to be up to 82 ± 4% (n=3) at best in low concentrations. The array of microchambers can be readily parallelized into a

large network (e.g. with a few thousand microchambers) without changing the processing time. Therefore, we can increase the volume of samples tested within the same 10-minute processing time. More importantly, with this method the initial sample does not need any dilution or preprocessing, which reduces the processing time.

2. Results and Discussion

2.1. Microfluidic Device and Procedure

The microfluidic device we designed consists of a micropatterned polydimethylsiloxane (PDMS) layer, fabricated using the soft-lithography technique and then plasma bonded to a glass slide. The PDMS layer featured parallel microchambers that are perpendicularly connected to longitudinal main channels by connecting channels. The device has two ports for sample loading and discharging. The schematic arrangement of the main channels and microchambers, along with scanning electron microscopy (SEM) and photographs of the device, are shown in Figures 1A and 1B.

The device was operated in three steps: First, a raw semen sample was loaded into the device by temporarily blocking the outlet (port -b) while the sample entered from the inlet (port a). Due to PDMS porosity, trapped air inside the microchambers was discharged, allowing the raw sample to fill them gradually. Second, the main channels were washed with a fresh medium. In this stage, the outlet was reopened and fresh medium was injected into the main channels, clearing them of all debris and non-viable sperm. Third, the fresh medium was gently injected from the inlet into the main channels and motile sperm were collected at the outlet. During the washing step, motile sperm naturally navigate along the microchamber walls (boundaries) that automatically guide them toward the main channels. Upon reaching the main and connecting channel intersections, motile sperm are washed away toward the outlet and collected. The collecting step continued until the majority of the motile sperm found their way out of the microchambers into the main channels. The operation steps are illustrated in Figure 1C.

To optimize our device, we investigated the impacts of channel depth and microchamber diameters on the loading capacity and separation performance of the device. In doing so, we varied the depth of the microchannels from 30 μm to 70 μm. In addition, we varied the microchamber diameters (350 μm, 500 μm, and 1000 μm) to evaluate the effects of boundary length on the separation performance of the device. Detailed illustrations of device dimensions can be found in Figure S1 and Table S1. Moreover, the increased area of gap size per volume implies more exposure of sperm to the outlet which increases efficiency of separation (Table S2).

It should be noted that the overall processing time remains the same even for increased volumes of samples resulting from increasing the number of microchannels and changing the channel depth. This consistency holds mainly because the collection time is a direct function of microchamber diameter and the time that a motile sperm takes to travel along its boundary to the exit (residence time). The time involved in the washing step is only a fraction of sperm residence time in the microchambers and does not significantly affect the total separation time.

Overall, operating the device is simple and requires only a syringe pump, a syringe for injecting fresh medium, and an Eppendorf tube in which to collect the motile sperm from the outlet, as illustrated in Figure 1D. Thus, this easy-to-operate, efficient, and high-throughput platform can offer an ideal and non-invasive alternative for separation of motile sperm needed for clinical and research studies.

2.2. Device Loading Time and Volume

As the microchamber diameter increases, the device loading time increases accordingly. Theoretically, the microchamber's loading time with a raw semen sample is a function of PDMS porosity, applied pressure(34) (or mass flow at the inlet), and microchamber volume. In the Supplemental Information (SI) section 3, we used a simplifying approximation and showed that the loading process can be theoretically modeled by a set of equations. A qualitative comparison of theory and experiment is shown in Supplementary Movie S1). In Figure 2,

sample progression inside the microchambers is visualized through time-lapse images. Dashed red lines represent the common interface of the sample and air trapped in the microchambers. The effects of three microchamber diameters (350 μm, 500 μm, and 1000 μm) and two flow rates (540 μL/h and 1240 μL/h) on loading time are shown in Figure S3. Consistently with our theoretical predictions, the experiments demonstrated an exponential correlation over time for loaded volume. In other words, the rate of loading is initially fast, but decreases as the loaded volume inside the microchambers increases, until each microchamber is fully loaded. More importantly, loading occurs simultaneously and almost uniformly for all the microchambers (as indicated by the narrow error bars in Figure S3). This feature gives us the ability to increase the number of microchambers to thousands to accommodate higher sample volumes while maintaining robust control over loading times.

2.3. Sperm Population Equilibrium in Microchambers

With successful loading of the raw semen sample into the device, motile sperm can be seen everywhere in the microchip including the microchambers and main channels. Given their motility, they move constantly from the main channel to the microchambers and vice versa. Such movements quickly settle into an equilibrium between the sperm that move into microchambers and those that leave it, resulting in an average motile sperm population inside the microchannels. Reaching this equilibrium is crucial as it later provides us with a high degree of flexibility in washing the main channel and removing all the debris (including motile and immotile sperm). We validated our hypothesis by observing an intersection of a connecting channel with the main channel, as demonstrated in Figure 3A. As can be seen in the time-lapse images, two spermatozoa enter and exit the microchamber (shown in red and green, respectively). The sperm trajectories in the vicinity of an intersection are demonstrated in Figure 3B, where purple dots represent sperm exiting the microchamber and red and blue dots represent sperm swimming toward the microchamber entrance from the right and left walls. Not all the sperm approaching the intersection enter the microchamber that is highlighted by

the intensity of the blue and red colors in the left part of Figure 3B. Darker colors represent sperm entering the microchamber and lighter colors represent sperm that are deflected from the connecting channel and do not enter it. Our results showed that nearly half of the sperm swimming from the left and right sides of the connecting channel entered the microchambers (dark blue and red dots in Figure 3B). This phenomenon occurs mainly because sperm that approach the intersection at a right angle will detach from the main channel wall at multiple deflection angles, resulting in swimming directions toward or away from the microchamber.(35, 36) Our measurements show that the deflection angle for the right and left swimmers are 22.19° (± 13.5°, n = 24) and 21.51° (± 13.2°, n = 21), respectively. These figures are consistent with the reported scattering data for the bull spermatozoa at 29 °C.(35) These results also show that a sperm deflection angle is independent of swimming direction, and that sperm populations entering from the right and left walls are almost equal. Further, sperm exiting the microchambers showed no directional preferences. In other words, sperm exiting the microchambers toward the front wall are equally likely to swim to the left or to the right. However, in human sperm there are other studies showing the deflection of sperm passing near corners which show the same pattern.(37) Last, the number of sperm approaching the intersection from the left or right is approximately the same. Our results show that this microchamber-based platform reaches a kinematic equilibrium state, in terms of sperm count in the microchambers, that is found to be highly persistent.

The difference between the cumulative population of sperm exiting a microchamber, and those entering it, remains constant for various concentrations of ~ 3 M mL^{-1} (1:10 dilution) to ~15 M mL^{-1} (1:1 dilution), over 100 seconds for concentrations of 1:1 and 1:3 dilution, and 200 seconds for 1:10 dilution. This indicates that this equilibrium state remains dominant over a long time (see Figures 3C–3E). The rate of sperm exchange between the microchambers and the main channels is shown in Figure 3F for three concentrations. This rate for small

concentrations (1:10) is low enough to provide an operator with ample time to prepare for the washing and collection steps without losing efficiency.

2.4. Extraction and Residence Time in the Collection Step

Motile sperm trapped inside the microchambers during the loading step actively interact with their surrounding boundary and swim toward it. Based on their incident angle with the microchamber wall, they navigate in a clockwise or counterclockwise manner along the boundaries(38) until they are guided toward the main channel. Upon entering the main channel, they are washed away with a flow of fresh medium, which is continuously injected. Hydrodynamics dictates that fresh medium flows only through the main channels where even higher injection flow rates do not disturb the quiescent conditions inside the microchambers (Figure 4A). This is important as it not only provides the right conditions for motile sperm navigation toward the washing flow but ensures the entrapment of immotile particles and sperm inside the microchambers. This is illustrated both experimentally and numerically using an injection flow rate of 10 μL/h from the main channel's inlet (left and right side insets, respectively, of Figure 4A).

Figure 4B shows the position of the immotile sperm loaded into a particular microchamber before and after washing and the collection step. As can be seen, the positions of dead sperm remain unchanged or only slightly changed by their interaction with motile sperm. The absence of motile sperm in the "before washing step" image (Figure 4B, left) is because motile sperm are present only along the walls of the microchamber that are under the halo-scattered light effect of microscopy. Supplementary Movie S2 clearly indicates the presence of motile sperm along the microchamber wall 10 seconds before washing.

Regarding the platform's efficiency, the concentration of motile sperm collected from the outlet is inversely correlated to the injection flow rate of the fresh medium. Higher injection flow rates do not improve performance and only reduce the final concentration of motile sperm due to the excessive amount of medium used during the washing step. The collected sperm

volume should not excessively exceed the initial loading volume of the raw sample; otherwise collected samples would be too diluted and require centrifugation. On the other hand, lower injection flow rates—below an optimum value—increase the chances of sperm rheotaxis (a behavior that is not desired) inside the main channels. With injection flow rates lower than sperm rheotaxis velocity, sperm can swim in the direction opposite to that of the injected medium and enter the adjacent microchambers, thus increasing the collection time as well as reducing microchip efficiency. Note that rheotaxis occurs only within a narrow range of mass flow rates and flow rates greater than this range overcome sperm's swimming force and easily drag them downstream.(13, 39) In this regard, we investigated, experimentally and numerically, the effects of flow rates on the rheotaxis of sperm exiting the microchambers. Figure 4C shows that the sperm trajectories are distorted by the medium flow at varying flow rates (Q = 1.9 μL/h and 0.7 μL/h) compared with what is shown in Figure 3B, which illustrates what happens when there is no flow. Dot trajectories of sperm swimming along the left wall of the connecting channel are shown in orange and those of sperm navigating near the right wall are shown in blue. A higher flow rate (i.e., Q = 1.9 μL/h) outweighs the sperm's motility and easily drags them toward the outlet, resulting in 100% recovery of sperm swimming out of microchambers after the start of the collection step. Conversely, sperm motility becomes significant with the lower flow rate (i.e. Q = 0.7 μL/h), such that sperm can swim upstream by alternating between the main channel walls in a butterfly-shaped trajectory, as reported previously.(16) Sperm swimming in such a pattern will find their way back to microchambers (Supplementary Movie S3).

For the numerical simulations shown in Figure 4C, we used a population of 40 sperm with normally distributed velocities. For initial conditions, we released half of the sperm from an arbitrary point near the right-hand wall and the other half from an arbitrary point near the left-hand wall in a direction perpendicular to the flow. We used turning dynamics in sperm swimming directions to calculate their 2D trajectories while they exit the microchambers and

are being exposed to the flow in the main channel.(13, 40) (Details regarding these simulations can be found in *SI section 4*).

Figure 4D facilitates comparison of cumulative sperm collection from the last microchamber (500μm in size) in a row of 48 microchambers with the total cumulative number of sperm, collected from that specific row. As is evident, 28 out of 36 sperm (~ 78%) are collected within 100 seconds and the remaining sperm need more than 200 seconds to exit the microchamber. A total of 655 sperm were collected in 300 seconds and the microchambers were checked afterwards to ensure that no swimming sperm remained in the microchambers. The samples are not homogeneous in terms of the number of sperm in the microchambers, meaning that several trials result in various numbers of sperm retrieved from a particular microchamber (*SI section 5*).

Residence times of loaded sperm vary based on their initial positions, velocity, swimming directions, the microchamber diameter, and the length of the connecting channels. For sperm swimming at the same velocity, the minimum and maximum residence times are observed with the sperm that move along the shortest and longest paths from their original positions inside a microchamber until they reach the intersections that connect the microchambers to the main channels.

Additionally, we neglected sperm–sperm interactions, assuming that the movement of one sperm does not affect the motion path of nearby sperm. We derived a formula for residence time distributions across a population of loaded sperm with respect to their velocity distribution. First, we considered a pool of sperm with Gaussian velocity distribution $<v, \sigma_v>$ loaded into a microchamber of a known diameter (D) and a connecting channel of a known length (L). The distribution of the residence time of this population can be described by Equation (1),

$$t = \frac{\pi D + 2L}{v}(pq + (1-p)(1-q)) \qquad (1)$$

where p is the uniformity of the initial sperm distribution on the microchambers' wall and q is another uniform random variable set to 1 for clockwise-swimming sperm (half of the

population) and 0 for counterclockwise-swimming sperm. It should be noted that our calculations were performed assuming that the system is at equilibrium, where most of the motile sperm have already reached the microchamber boundaries (additional discussion of this topic can be found in *SI section 5*). Notice that this equation does not consider sperm collisions on the boundaries and assumes continuous sperm navigation along the boundaries upon their arrival at any contact angle. The residence times for all of the designs were calculated for a sperm population of v=80 μm/s and σ_v =20 μm/s.

Theoretical and experimental data are plotted and shown in Figure 5. The measured residence times resemble a left-skewed distribution and are in accordance with theoretically predicted values. In addition, the change in residence times is more noticeable as microchamber diameters widen. Deviation of the predicted results (based on the model) from the experimental results is more significant for larger microchambers. We think this is due mainly to the fact that, as the microchamber diameter increases, so do the sperm–sperm interactions, which we assumed to be insignificant in our model. It is also clear that the residence times are independent of the microchamber depth, because of sperm accumulation on the top and bottom surfaces of the microchip and their preference for 2D navigation near top and bottom surfaces.(41, 42) The collection time for more than 90% of the sperm in the microchambers were 60, 135, and 215 seconds for microchambers with diameters of D = 350, 500, and 1000 μm, respectively, and did not vary substantially when we increased the microchip depth from 30 μm to 70 μm.

2.5. Characteristics of the Collected Sperm

2.5.1. Motility

Before the extraction of sperm from the device they are collected in a collection zone. The collection zone lies immediately before the outlet of the microchip (red rectangle in Figure 6A and supplementary Movie S4). Channel width expansion in this area reduces medium flow velocity significantly, causing sperm to undergo rheotaxis, although they are not strong enough to return to the main channels. The concentration and motility percentage of the motile sperm

are evaluated after 5 minutes in this area under various designs. The results are shown in Figures 6B and 6D for a motile sperm sample of concentration 5.9 ± 0.7 M mL^{-1} and in Figures 6C and 6E for a motile sperm sample of concentration 2.4 ± 0.3 M mL^{-1}. In higher concentration of raw sample, the concentration and motility percentage in the collection zone increased substantially. For lower concentration in 500 μm microchambers, the concentration in the collection zone rose as high as in the raw sample but far less than in 1000 μm microchambers. This difference reflects the fact that the design capacity of the 500 μm microchambers is half that of the 1000 μm microchambers but the volume of the collection zone under both designs is approximately the same. Therefore, there is not enough motile sperm in the loaded sample to increase the concentration in the collection zone with a diameter of 500 μm in lower concentrations. The depth of the channel, however, did not affect the results.

Following the collection process, the inlet flow rate is increased so that all the sperm in the collection zone are pushed to the outlet and collected in the collection tube (extraction). We further analyzed the extracted progressive sperm by measuring and comparing their straight-line velocities (VSLs) and average-path velocities (VAPs), as shown in Figure 6F. The resulting mean value of the VAP and VSL (Figure 6G) shows a significant increase in the mean VAP from 57 ± 10 μm/s in raw semen sample to 81 ± 13 μm/s in the extract, which is a result of the higher concentration of highly progressively motile sperm in the separated sample (Supplementary Movie S5).

In the case of oligozoospermia and asthenozoospermia, the concentration and progressive motility is low (<15 M mL^{-1} and <32% motility).(43) It is crucial to increase the efficiency of separation so that more sperm can be selected from a given sample to increase the chance of selecting the best sperm. The concentration of the sample of extracted sperm is shown in Figure 6H to be 3.2 ± 0.2 M mL^{-1}, with 90% motility, while the concentration in the raw sample is 8.5 ± 0.5 M mL^{-1}, with 38% motility. Given that 22.5 μL is loaded and 25 μL is extracted, roughly 75% of the motile sperm are collected (the equivalent of 5.2 × 10^4

spermatozoa). The motility of the separated sample is 90%, which means the motility percentage does not change after extraction relative to motility in the collection zone. The remaining sperm might not have sufficient progressive motility (Figure S7) or were likely withdrawn in waste removal.

We also studied the effects of microchamber diameter on the retrieval efficiency, as shown in Figures 6I and 6J at a depth of 30 μm. To test the efficiency of these devices, we used raw semen samples at a concentration of ~8.2 M mL^{-1} (21% motility). The collected extracts from the 1000 μm and 500 μm devices exhibited approximately 80% retrieval of the motile sperm from the initial sample loaded in the microchambers (Figure 6J). The retrieval efficiency was only 36 ± 16% for the smallest device with the smallest-diameter (350 μm). The low retrieval efficiency for the 350 μm device reflects the short residence time of the sperm in the microchambers. In other words, more than 50% of sperm exit the microchambers in less than 10–15 seconds during washing the waste from the main channels. For devices with larger microchambers (i.e., 1000 μm and 500 μm), the short initial washing steps for evacuating the waste from the main channels did not have a significant effect on final motile sperm concentration (for additional details on the experiment, please see the experimental section).

2.5.2. DNA Integrity

The Acridine Orange (AO) tests showed the sperm in the collection zone have higher green fluorescence signal compared to the sperm remaining in the microchambers after separation (Figure 7A). We examined the DNA fragmentation of the raw and extracted sperm from D = 1000 μm device for raw sperm with different level of DNA fragmentation index (DFI).(44) We created samples of various DFI by dilution of a regular sample with various ratios of a fragmented DNA sample. The fragmented DNA sample was produced by dipping a thawed sample into a 90 °C oil bath for 2 minutes to insure deceased motility. Figure 7B shows the DFI distribution, along with Red and Green Signals of the various dilutions and the corresponding separated samples. DNA integrity is shown in the Figure 7C. For the raw unseparated sample,

the DNA integrity was 70%, while for the separated sperm the DNA integrity was 93%. Further, in the case where the DNA integrity was low to begin with, the separated sperm exhibited a DNA integrity of 78%. In both cases the separated sperm showed 20% or higher DNA integrity than the bulk sample. This shows that the platform is reliable in separating motile sperm with lower DFI translating to higher quality.

Furthermore, our proposed microfluidic platform effectively differentiates and separates progressive and nonprogressive sperm. Our observations of a microchamber after 15 minutes revealed the formation of moon-like crater-shaped hollows as a result of the circular motion of nonprogressive sperm. The circular movement of nonprogressive sperm pushes the debris (egg-yolk extender particles) toward the microchamber walls and randomly creates hollow patterns inside the microchamber (Figure S7). This fact combined with the absence of any circular motion within the collected sample indicates that our platform can separate progressively motile sperm from the initial raw sample and trap nonprogressive sperm in the microchambers.

3. Conclusion

We propose a new microchamber-based microfluidics platform for targeted separation of progressively motile sperm directly from a raw semen sample in a short period of time (~10 minutes) with 75% separation efficiency. The loading of raw semen samples into microchambers and the subsequent retrieval of motile sperm are straightforward and require no special skills. Once the raw semen sample, without pre-treatment, is loaded, the microchip reaches a kinematic equilibrium state in terms of the number of sperm that enter or exit the microchambers. The equilibrium state further provides users with flexibility and controllability in the process as sufficient time remains for performing the rest of the operations. We evaluate the efficiency of our device by investigating the quality of motile sperm based on VSL and VAP measurements. The VAP and VSL of the separated sample show significant improvement over the raw sample—from 57 ± 13 and 51 ± 11 μm/s to 68 ± 10 and 81 ± 10 μm/s, respectively

($P < 0.05$). Moreover, AO analysis showed nearly 20% increase in DNA integrity of the separated sperm over raw samples in the range of 45% to 70% DNA integrity.

The pressure used for the loading was not high enough to induce detectable deformation to the PDMS and it was used only in a short period of time to be effective on sperm quality. The pressures of 10-40 MPa has been reported as sublethal range for sperm which is far beyond the yield stress of our PDMS device (1-2 MPa).(45) More importantly, intactness of the DNA of the cells combined with their higher motility ensures that the applied pressure in the loading step does not inflict any significant damage on the sperm cells.

We also measured and predicted sperm residence time inside the microchambers as well as the time needed to complete the entire progressive sperm collection process, which in both cases was no longer than 5 minutes. In addition, we showed that the microfluidic platform not only can separate motile sperm from immotile sperm but can also effectively differentiate and separate progressive sperm from nonprogressive sperm. Moreover, we optimized the concentration of the collected progressive sperm from a 38% motile raw sample of 8.5 M mL^{-1} to 2.3 M mL^{-1} with 90% motility by tuning the washing flow rate above the sperm's ability to exhibit rheotaxis. This is equivalent to separating 5.2×10^4 spermatozoa in only 10 minutes. This renders the platform suitable for low-concentration and low-progressive sperm cases (oligozoospermia and asthenozoospermia). This 384-microchamber platform can be easily extended to several thousand and the height of the microchambers can be increased to interrogate higher volumes of raw semen to separate more sperm without increasing the processing and separation time. Finally, we believe that our microfluidic platform can provide an ideal alternative to conventional sperm separation techniques and may contribute to improving diagnostics and ART outcomes for animal and human fertility.

4. Experimental Section

Commercially available cryopreserved bovine semen samples were generously donated by GENEX from URUS holding company, Ithaca, NY, USA. These samples were from a six-year old, mature black and white Holstein bull. The ejaculate concentration was ~ 2.9 billion cells/mL with pre-freeze motility of 65%. Frozen straws of bovine semen in egg-yolk extender were thawed by immersing them in a water bath at 37°C for 30–45 seconds immediately after being retrieved from a liquid nitrogen tank. The thawed semen were then transferred to 1.5 mL Eppendorf tubes. Fresh medium at 37°C was then added to the sample for viability. For experiments that needed low-concentration samples, fresh medium was used in the corresponding ratios. The samples were placed under the microscope stage for processes requiring less time than 5 minutes. For assays requiring more than 5 minutes to complete, a warm plate was used to ensure the viability of the sperm at 37°C and in the meantime the entire thawed sperm sample was kept on the warm plate at 37°C.

The sperm samples were treated by Tyrode's albumin lactate pyruvate (TALP) as a fresh medium. TALP was prepared using NaCl (110 mM), KCl (2.68 mM), NaH_2PO_4 (0.36 mM), $NaHCO_3$ (25 mM), $MgCl_2$ (0.49 mM), $CaCl_2$ (2.4 mM), HEPES buffer (25 mM), glucose (5.56 mM), pyruvic acid (1.0 mM), penicillin G (0.006% or 3 mg/500 mL), and bovine serum albumin (20 mg/mL) as the base solution to prepare the experimental buffer pH = 7.47.

The microfluidic chips were made of SU-8 and photolithography and poured Polydimethylsiloxane (PDMS) on the resulting mold as in conventional soft lithography. Syringe pumps (New Era) were used to load the samples into the microchambers at varying injection flow rates of 0.54 mL/h and 1.24 mL/h.

A Nikon eclipse TE3000 phase-contrast microscope was used to visualize the movement of the sperm in the channels. Movie recordings were acquired at 10 frames per second with a 20× objective and ANDOR Zyla 4.2 sCMOS digital camera. During the experiments, the microfluidic chip was kept on a heated 37 °C plate under a stereo microscope for experiments that required more than 5 minutes to complete. The VAP and VSL of the sperm were determined

using ImageJ (version 1.52a; NIH) and the resulting dot trajectories of the sperm were analyzed by Python 3.8. The VAP and VSL measurements were performed on samples in a microfluidics chip at 30 μm depth and 3-4 μL capacity to avoid the effects of channel height on sperm velocity previously reported by simulations and theoretical studies. In each experiment, 100 sperm were tracked.

Fluorescent microparticles were used to produce the image of the streamlines in the main channel.

Simulations were performed in COMSOL Multiphysics 5.4a for calculating the velocity field and shear rate. Particle-tracing physics were combined with laminar flow to track the sperm's 2D theoretical trajectories for two flow rates (0.7 and 1.9 μL/h), making it possible to optimize the flow rate and investigate rheotaxis effects. The simulated streamlines were also captured by a 10 μL/h flow rate in a layout corresponding to our geometry.

Extraction efficiencies are rated in devices with two rows of 38, 29, and 18 microchambers for diameters of 350, 500, and 1000 μm, respectively. The numbers above each line in Figure 6I represent the corresponding total volumes of microchambers (V) in each design. The efficiency—the ratio of total extracted sperm (N) to motile sperm in volume V—is then calculated. Therefore, by knowing the motile sperm concentration (α):

$$efficiency = \frac{N}{\alpha V} \times 100\ \%, \qquad (2)$$

In evaluating efficiency in 384-microchamber platform V is chosen as total volume of the chip (22.5 μL). The experiments involving separation of sperm in the collection zone were conducted only for 500 and 1000 μm diameter (D) microchamber designs with 812 microchambers (14 rows of 58 microchambers) and 384 microchambers (8 rows of 48 microchambers), respectively. Each design was manufactured at both 30 and 70 μm depths with the same masks.

The extraction experiments (Figures 6F-6H) were conducted only in D = 1000 μm and depth of 70 μm devices with 384 microchambers (21 μL) because the loaded volumes in other devices that were below 10 μL in capacity, resulted in handling problems. (The capacity of the

D = 500 μm with depth 70 μm was 11 μL in 812 microchambers and the separated sperm sample had a smaller volume than 10 μL therefore it was difficult to transfer to other microchip for analysis.) After loading the chip and removing the waste, TALP was injected from the inlet at a 40 μL/h flow rate for 5 minutes (this design has 9 parallel rows of main channels, as can be seen in Figures 1B and 6A). The flow rate was then increased to 10 mL/h for ~7 seconds to extract the sperm in the collection zone from the chip in the collection tube (approximately 25 μL was collected each time). The collected samples were then transferred to a 30 μm-high channel to measure VAP and VSL, as mentioned earlier.

AO test was performed with a slight modification of the method described elsewhere (44) and DFI more than 0.15 was categorized as a DNA fragmented cell. A solution containing 2.0 ml 2.0 M HCl, 0.439 g NaCl, and 0.05 ml Triton X-100 was prepared in sufficient DI water to achieve a volume of 50 ml, the pH was adjusted to 1.2 with 5.0 M HCl. An air dried glass smear of sperm were immersed in the solution for 30 seconds and then washed with ethanol and air dried. To 500 mL of DI water was added 3.8869 g (0.020 mol) citric acid monohydrate, 8.946 g (0.063 mol) sodium phosphate dibasic (Na_2HPO_4), 186 mg (6.36×10^{-4} mol) EDTA disodium and 4.385 g (0.075 mol) NaCl and was stirred overnight to ensure that the EDTA is entirely dissolved in this staining buffer. The pH was adjusted to 6.0 with concentrated NaOH solution. To 20 mL of DI water was added 20 mg (4.83×10^{-5} mol) of Acridine Orange hemi (zinc chloride) salt, the solution was stirred to dissolve the powder. To 50 mL of staining buffer, 300 μL of AO solution was added and the glass slides were immersed in this staining solution for 3 minutes. After which time the remaining stain was washed with ethanol. All the fluorescent images were captured in a dark room with exposure time of 300 ms since AO solution is very sensitive to light. Red and green signal of more than 200 sperm were evaluated and DFI was calculated as

$$DFI = \frac{Red}{Red + Green} \qquad (3)$$

The python code that was used to evaluate the DNA integrity has been uploaded online.(46) For the sperm staining in the microchambers and collection zone, after 4 minutes the separation process was terminated and the chip was allowed to gradually dry out over the period of one day. After which the PDMS was peeled off the glass slide and the chip was stained as above. Statistical analyses were performed using MATLAB and one-way analyses of variance. Each experiment was repeated three times and values were reported as mean ± standard deviations (error bars). The number of data points are revealed whenever necessary in parentheses.

Acknowledgments

We would like to thank Farhad Javi for setting up the fluorescent particles to facilitate visualization of the streamlines in the main channels, and Ann V. Nguyen and especially Kelley J. Donaghy for scientific writing and editing support. The manufacturing process involving the microfluidic platform was performed at the Cornell Nanoscale Facility (CNF), a member of the National Nanotechnology Coordinated Infrastructure (NNCI), which is supported by National Science Foundation Grant ECCS-1542081.

References

1. Nosrati R, Graham PJ, Zhang B, Riordon J, Lagunov A, Hannam TG, et al. Microfluidics for sperm analysis and selection. Nature Reviews Urology. 2017;14(12):707.
2. Sakkas D. Novel technologies for selecting the best sperm for in vitro fertilization and intracytoplasmic sperm injection. Fertility and sterility. 2013;99(4):1023-9.
3. Evenson D, Darzynkiewicz Z, Melamed M. Relation of mammalian sperm chromatin heterogeneity to fertility. Science. 1980;210(4474):1131-3.
4. Sakkas D, Ramalingam M, Garrido N, Barratt CL. Sperm selection in natural conception: what can we learn from Mother Nature to improve assisted reproduction outcomes? Human reproduction update. 2015;21(6):711-26.
5. Bartoov B, Berkovitz A, Eltes F. Selection of spermatozoa with normal nuclei to improve the pregnancy rate with intracytoplasmic sperm injection. New England Journal of Medicine. 2001;345(14):1067-8.
6. Schinfeld J, Sharara F, Morris R, Palermo GD, Rosenwaks Z, Seaman E, et al. Cap‐Score ™ prospectively predicts probability of pregnancy. Molecular reproduction and development. 2018;85(8-9):654-64.
7. Marzano G, Chiriacò MS, Primiceri E, Dell'Aquila ME, Ramalho-Santos J, Zara V, et al. Sperm selection in assisted reproduction: A review of established methods and cutting-edge possibilities. Biotechnology Advances. 2020:107498.
8. Suarez S. How do sperm get to the egg? Bioengineering expertise needed! Experimental mechanics. 2010;50(9):1267-74.

9. Suarez SS, Pacey A. Sperm transport in the female reproductive tract. Human reproduction update. 2006;12(1):23-37.
10. Muratori M, Tarozzi N, Carpentiero F, Danti S, Perrone F, Cambi M, et al. Sperm selection with density gradient centrifugation and swim up: effect on DNA fragmentation in viable spermatozoa. Scientific reports. 2019;9(1):7492.
11. Shirota K, Yotsumoto F, Itoh H, Obama H, Hidaka N, Nakajima K, et al. Separation efficiency of a microfluidic sperm sorter to minimize sperm DNA damage. Fertility and sterility. 2016;105(2):315-21. e1.
12. Saylan A, Erimsah S. High quality human sperm selection for IVF: A study on sperm chromatin condensation. Acta histochemica. 2019;121(7):798-803.
13. Zaferani M, Cheong SH, Abbaspourrad A. Rheotaxis-based separation of sperm with progressive motility using a microfluidic corral system. Proceedings of the National Academy of Sciences. 2018;115(33):8272-7.
14. Asghar W, Velasco V, Kingsley JL, Shoukat MS, Shafiee H, Anchan RM, et al. Selection of functional human sperm with higher DNA integrity and fewer reactive oxygen species. Advanced healthcare materials. 2014;3(10):1671-9.
15. Chinnasamy T, Kingsley JL, Inci F, Turek PJ, Rosen MP, Behr B, et al. Guidance and Self‐Sorting of Active Swimmers: 3D Periodic Arrays Increase Persistence Length of Human Sperm Selecting for the Fittest. Advanced Science. 2018;5(2):1700531.
16. Zaferani M, Palermo GD, Abbaspourrad A. Strictures of a microchannel impose fierce competition to select for highly motile sperm. Science advances. 2019;5(2):eaav2111.
17. Cho BS, Schuster TG, Zhu X, Chang D, Smith GD, Takayama S. Passively driven integrated microfluidic system for separation of motile sperm. Analytical chemistry. 2003;75(7):1671-5.
18. Nosrati R, Vollmer M, Eamer L, San Gabriel MC, Zeidan K, Zini A, et al. Rapid selection of sperm with high DNA integrity. Lab on a Chip. 2014;14(6):1142-50.
19. Mokhtare A, Xie P, Abbaspourrad A, Rosenwaks Z, Palermo GD. EMBRYOLOGY LAB-ON-A-CHIP: AUTOMATED OOCYTE DENUDATION MICROFLUIDIC DEVICE. Fertility and Sterility. 2020;114(3):e76.
20. Mokhtare A, Xie P, Abbaspourrad A, Rosenwaks Z, Palermo G, editors. Toward an ICSI chip: automated microfluidic oocyte denudation module. HUMAN REPRODUCTION; 2020: OXFORD UNIV PRESS GREAT CLARENDON ST, OXFORD OX2 6DP, ENGLAND.
21. Kashaninejad N, Shiddiky MJA, Nguyen NT. Advances in Microfluidics‐Based Assisted Reproductive Technology: From Sperm Sorter to Reproductive System‐on‐a‐Chip. Advanced Biosystems. 2018;2(3):1700197.
22. Seo D-b, Agca Y, Feng Z, Critser JK. Development of sorting, aligning, and orienting motile sperm using microfluidic device operated by hydrostatic pressure. Microfluidics and Nanofluidics. 2007;3(5):561-70.
23. Denissenko P, Kantsler V, Smith DJ, Kirkman-Brown J. Human spermatozoa migration in microchannels reveals boundary-following navigation. Proceedings of the National Academy of Sciences. 2012;109(21):8007-10.
24. Nosrati R, Graham PJ, Liu Q, Sinton D. Predominance of sperm motion in corners. Scientific reports. 2016;6:26669.
25. Schuster TG, Cho B, Keller LM, Takayama S, Smith GD. Isolation of motile spermatozoa from semen samples using microfluidics. Reproductive biomedicine online. 2003;7(1):75-81.
26. Gai J, Nosrati R, Neild A. High DNA integrity sperm selection using surface acoustic waves. Lab on a Chip. 2020.
27. Phiphattanaphiphop C, Leksakul K, Phatthanakun R, Khamlor T. A novel microfluidic chip-based sperm-sorting device constructed using design of experiment method. Scientific reports. 2020;10(1):1-13.

28. Zhang Z, Liu J, Meriano J, Ru C, Xie S, Luo J, et al. Human sperm rheotaxis: a passive physical process. Scientific reports. 2016;6:23553.
29. Nagata MPB, Endo K, Ogata K, Yamanaka K, Egashira J, Katafuchi N, et al. Live births from artificial insemination of microfluidic-sorted bovine spermatozoa characterized by trajectories correlated with fertility. Proceedings of the National Academy of Sciences. 2018;115(14):E3087-E96.
30. Tasoglu S, Safaee H, Zhang X, Kingsley JL, Catalano PN, Gurkan UA, et al. Exhaustion of racing sperm in nature‐mimicking microfluidic channels during sorting. Small. 2013;9(20):3374-84.
31. Matsuura R, Takeuchi T, Yoshida A. Preparation and incubation conditions affect the DNA integrity of ejaculated human spermatozoa. Asian journal of andrology. 2010;12(5):753.
32. Matsuura K, Uozumi T, Furuichi T, Sugimoto I, Kodama M, Funahashi H. A microfluidic device to reduce treatment time of intracytoplasmic sperm injection. Fertility and sterility. 2013;99(2):400-7.
33. Palermo GD, Neri QV, Cozzubbo T, Rosenwaks Z. Perspectives on the assessment of human sperm chromatin integrity. Fertility and sterility. 2014;102(6):1508-17.
34. Guo W, Teo AJ, Gañán-Calvo AM, Song C, Nguyen N-T, Xi H-D, et al. Pressure-Driven Filling of Closed-End Microchannel: Realization of Comb-Shaped Transducers for Acoustofluidics. Physical Review Applied. 2018;10(5):054045.
35. Kantsler V, Dunkel J, Polin M, Goldstein RE. Ciliary contact interactions dominate surface scattering of swimming eukaryotes. Proceedings of the National Academy of Sciences. 2013;110(4):1187-92.
36. Rode S, Elgeti J, Gompper G. Sperm motility in modulated microchannels. New Journal of Physics. 2018.
37. Bukatin A, Denissenko P, Kantsler V. Self-organization and multi-line transport of human spermatozoa in rectangular microchannels due to cell-cell interactions. Scientific Reports. 2020;10(1):1-8.
38. Guidobaldi A, Jeyaram Y, Berdakin I, Moshchalkov VV, Condat C, Marconi VI, et al. Geometrical guidance and trapping transition of human sperm cells. Physical Review E. 2014;89(3):032720.
39. Miki K, Clapham DE. Rheotaxis guides mammalian sperm. Current Biology. 2013;23(6):443-52.
40. Bukatin A, Kukhtevich I, Stoop N, Dunkel J, Kantsler V. Bimodal rheotactic behavior reflects flagellar beat asymmetry in human sperm cells. Proceedings of the National Academy of Sciences. 2015;112(52):15904-9.
41. Berke AP, Turner L, Berg HC, Lauga E. Hydrodynamic attraction of swimming microorganisms by surfaces. Physical Review Letters. 2008;101(3):038102.
42. Su T-W, Xue L, Ozcan A. High-throughput lensfree 3D tracking of human sperms reveals rare statistics of helical trajectories. Proceedings of the National Academy of Sciences. 2012;109(40):16018-22.
43. Esteves SC, Roque M, Bedoschi G, Haahr T, Humaidan P. Intracytoplasmic sperm injection for male infertility and consequences for offspring. Nature Reviews Urology. 2018;15(9):535.
44. Wang Y, Riordon J, Kong T, Xu Y, Nguyen B, Zhong J, et al. Prediction of DNA Integrity from Morphological Parameters Using a Single‐Sperm DNA Fragmentation Index Assay. Advanced Science. 2019.
45. Pribenszky C, Horváth A, Végh L, Huang SY, Kuo YH, Szenci O. Stress preconditioning of boar spermatozoa: a new approach to enhance semen quality. Reproduction in Domestic Animals. 2011;46:26-30.
46. Yaghoobi M, Abbaspourrad A. Manual Evaluation of Sperm DNA Fragmentation. 1.0 ed: GitHub; 2021.

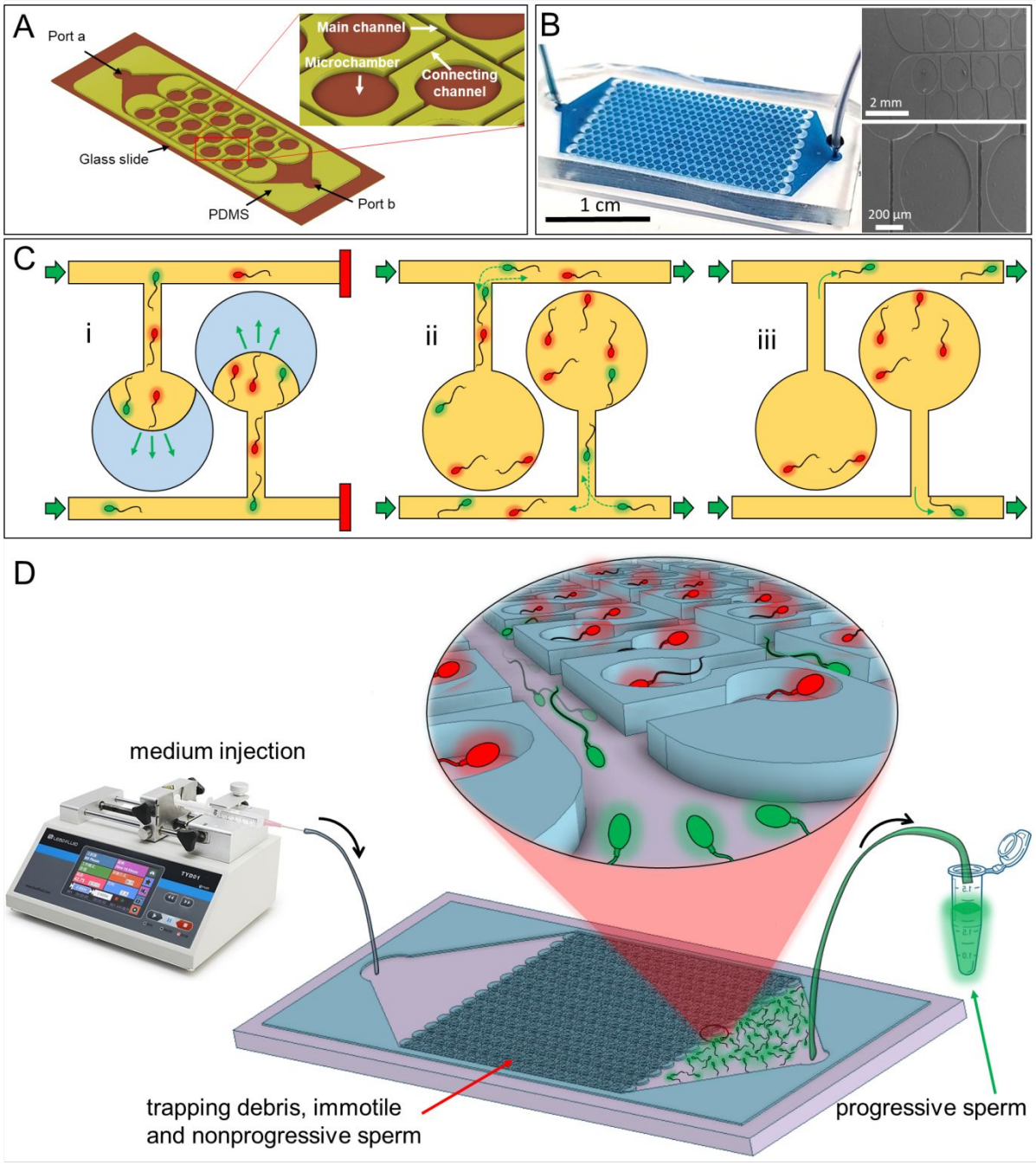

Figure 1. (A) Schematic representation of the platform design for sperm separation. (B) Photograph of microchambers filled with blue dye and SEM image of the microchambers. (C) (i) Loading the semen sample into the microchambers and discharging air that is trapped by the porosity of PDMS under constant pressure (red bar indicated closed channels); (ii) washing the main channel for sperm collection and (iii) collecting the washed, progressively motile sperm.

(D) The parallelization capacity of the platform for increasing the volume of loaded samples and simplifying the collection process.

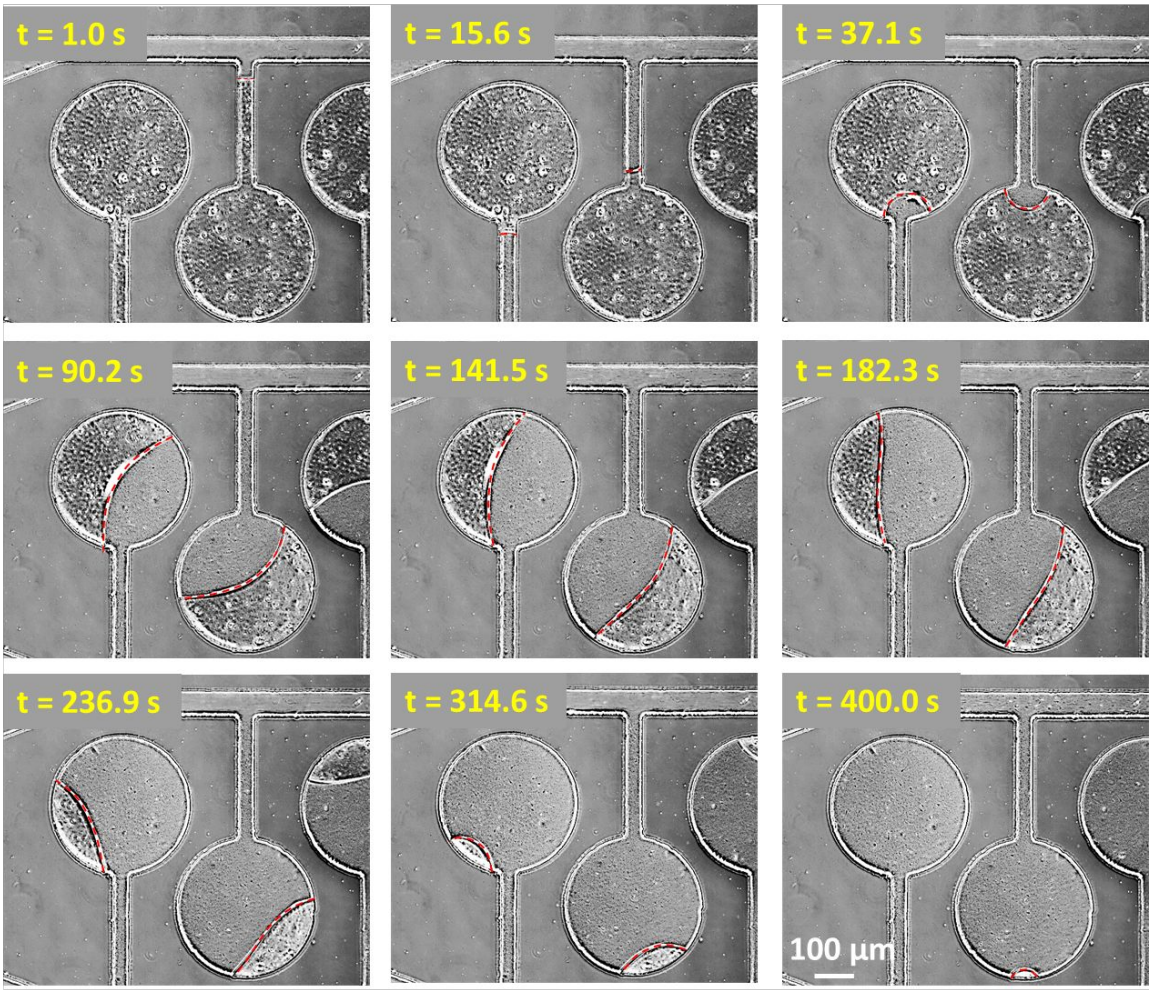

Figure 2. The loading process for microchambers with diameter 350 µm (*D*) and 70 µm (*H*). The common interface of the sperm sample and the air trapped in the channel (dashed red line) is attenuated in each time-lapse image. This experiment was performed by applying constant pressure on the sample loaded into the chip while the outlet of the main channel is closed.

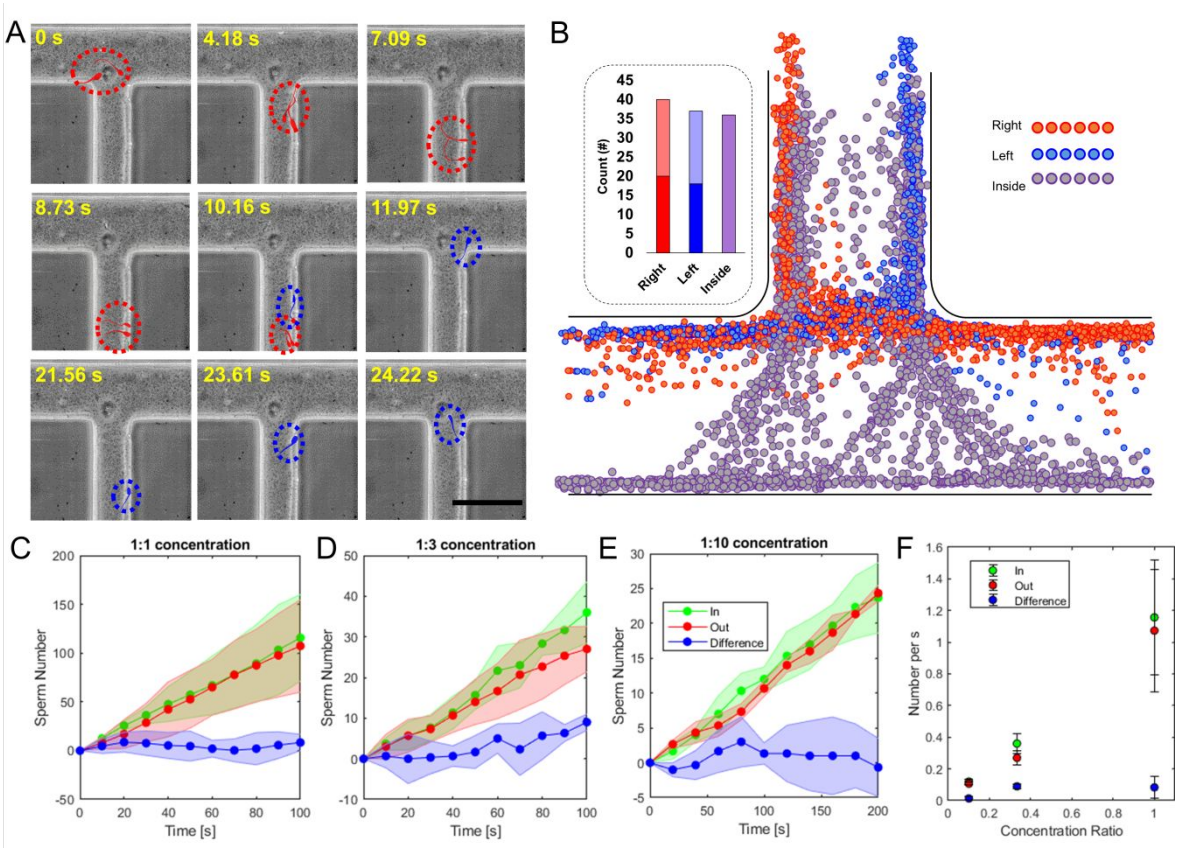

Figure 3. The overall number of sperm in the microchambers remains constant. (A) Several time-lapse images of a typical junction in the equilibrium state show two spermatozoa entering the channel (highlighted in red and enclosed by red dashed ovals) and two other spermatozoa exiting (highlighted in blue and enclosed in blue dashed ovals) over the course of 24 seconds. The scale bar represents 100 μm. (B) Dot trajectories of sperm swimming near the junction wall from the right (red dots) and the left (blue dots) and those exiting the microchamber swimming near the connecting channel walls (purple dots). Numbers of these sperm are shown in the left diagram in the same color codes. The light blue and red colors indicate sperm that enter the microchamber from the right and the left, respectively. (C-E) Cumulative numbers of sperm entering and exiting a microchamber for varying concentrations (n = 3). (F) Cumulative number of sperm for varying concentration ratios over 100-second periods (n = 3).

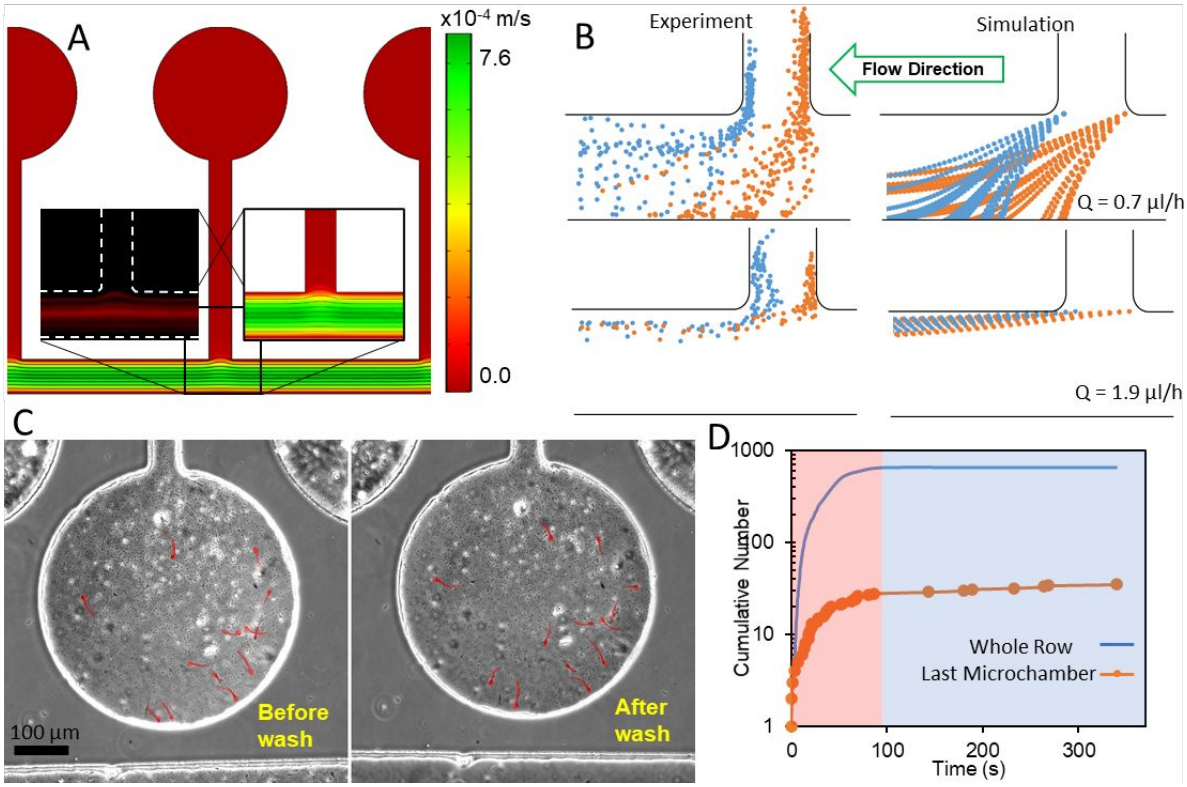

Figure 4. Washing steps and sperm extraction. (A) Streamlines and the velocity magnitude in the main channel for a volume flow rate of 10 µL/h. The streamlines of the magnified region are shown experimentally with fluorescent particles. (B) Dead sperm and particles remain in the microchamber. The dead sperm are highlighted in red. (C) Rheotaxis for both simulation and experiments; the rheotaxis of motile sperm can be seen in Supplementary Movie S2 for both conditions. (D) Typical extraction diagram of the device over time for D = 500 µm and depth of 30 µm of the last microchamber in a row and for the entire number of sperm in that row.

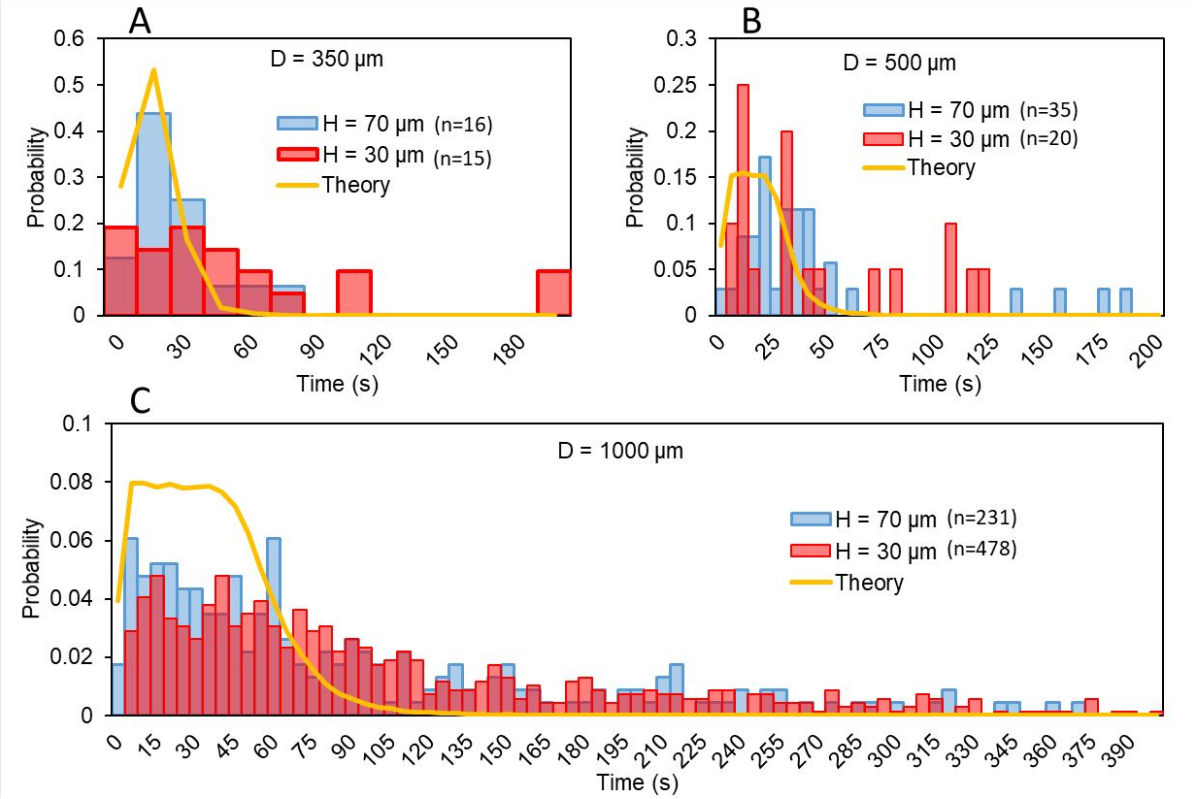

Figure 5. The distribution of residence times of sperm in microchambers of varying diameters and at 30 µm and 70 µm depths (the theoretical distribution is also shown for comparison purposes).

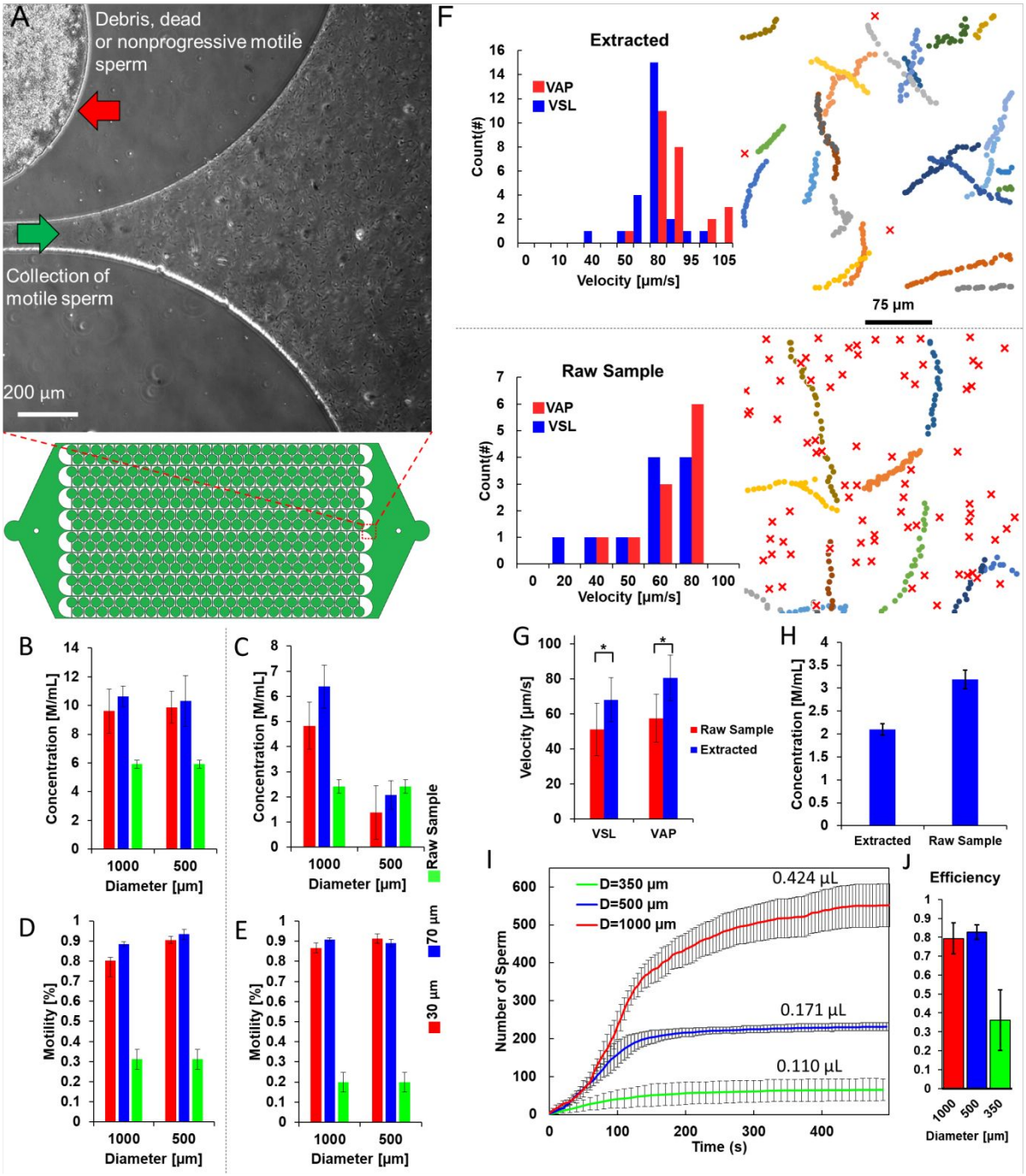

Figure 6. Bulk separation of motile sperm. (A) The population of the sperm at the outlet is visible (the zoomed-out red rectangle represents the collection zone). (B-E) Motile concentrations and motility percentages of the sperm collected in collection zones and raw samples at diameters of 1000 µm and 500 µm and at depths of 30 and 70 µm using two concentrations: B and D show results with the higher concentration of starting raw sample and C and E show results with the lower concentration. (F) Velocity distribution (VAP and VSL)

of the extracted population of sperm from the device and raw sample. The trajectories of motile sperm are shown in separate colors and dead sperm are indicated by red crosses. (Debris that is present in the frozen thawed sample of bovine semen is also filtered out through the device and cannot be seen in the separated sample.) (G) Mean VAP and VCL of extracted and raw sample (* $p < 0.05$, $n = 3$). (H) Motile concentration of extracted and raw sample from a device with $D = 1000$ μm and depth 70 μm ($n = 3$). (I, J) Efficiency of the extraction from microchamber of varying diameters at a depth of 30 μm.

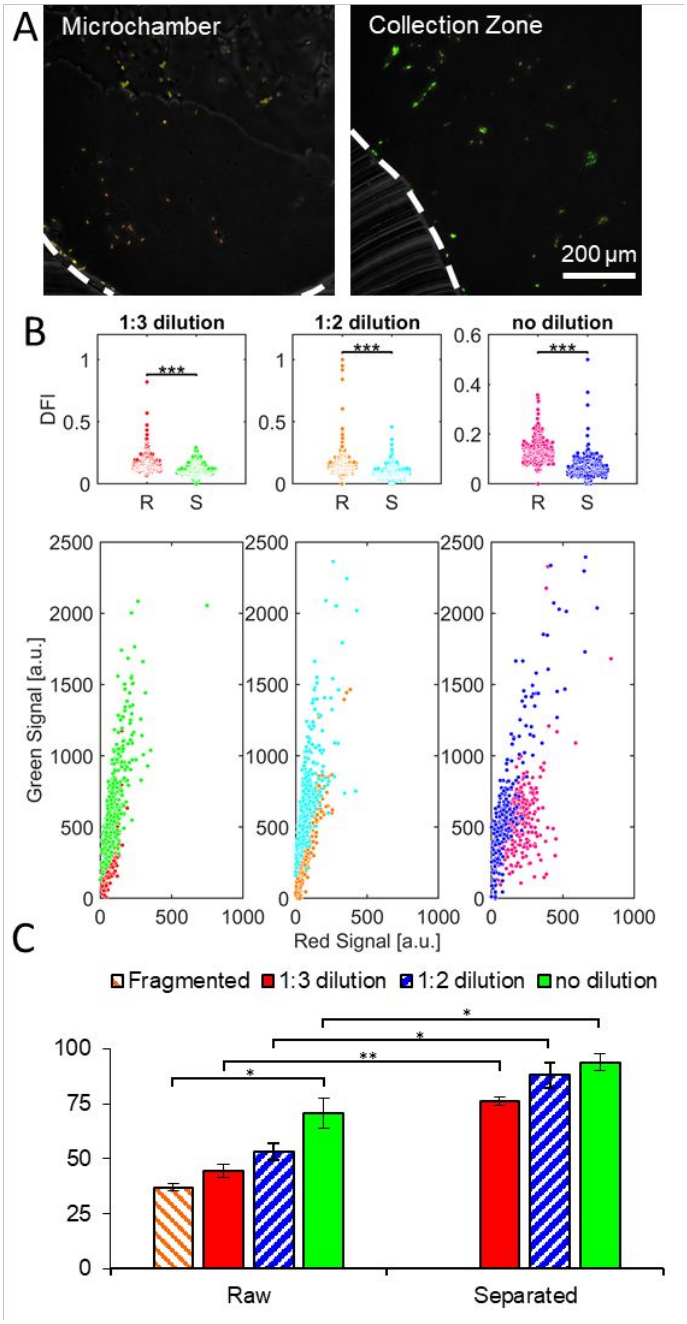

Figure 7. DNA integrity of collected and extracted sperm. (A) Sperm remaining in the microchambers after the separation showed significant DNA damage compared to sperm in the collection zone. White dashed lines show the microchannels boundaries. (B) DFI distribution (n > 200 sperm) of the loaded and separated sperm of the three experiments; 1:3, 1:2 and zero dilution of raw sample with Fragmented DNA samples. (*** $p < 0.00001$, ** $p < 0.01$, * $p < 0.05$) R and S are raw and separated samples, respectively. (C) DNA integrity of the raw and separated sperm of the experiments in (B).